Langmuir

Letter

pubs.acs.org/Langmuir

Experimental Investigation of Optimal Adhesion of Mushroomlike Elastomer Microfibrillar Adhesives

Hamidreza Marvi,[†,‡] Sukho Song,[†,§] and Metin Sitti*[,†,§]

[†]Carnegie Mellon University, Pittsburgh, Pennsylvania 15213, United States

[‡]Arizona State University, Tempe, Arizona 85287, United States

[§]Max-Planck Institute for Intelligent Systems, Stuttgart 70569, Germany

ABSTRACT: Optimal fiber designs for the maximal pull-off force have been indispensable for increasing the attachment performance of recently introduced gecko-inspired reversible micro/nanofibrillar adhesives. There are several theoretical studies on such optimal designs; however, due to the lack of three-dimensional (3D) fabrication techniques that can fabricate such optimal designs in 3D, there have not been many experimental investigations on this challenge. In this study, we benefitted from recent advances in two-photon lithography techniques to fabricate mushroomlike polyurethane elastomer fibers with different aspect ratios of tip to stalk diameter (β) and tip wedge angles (θ) to investigate the effect of these two parameters on the pull-off force. We found similar trends to those predicted theoretically. We found that β has an impact on the slope of the force−displacement curve while both β and θ play a role in the stress distribution and crack propagation. We found that these effects are coupled and the optimal set of parameters also depends on the fiber material. This is the first experimental verification of such optimal designs proposed for mushroomlike microfibers. This experimental approach could be used to evaluate a wide range of complex microstructured adhesive designs suggested in the literature and optimize them.

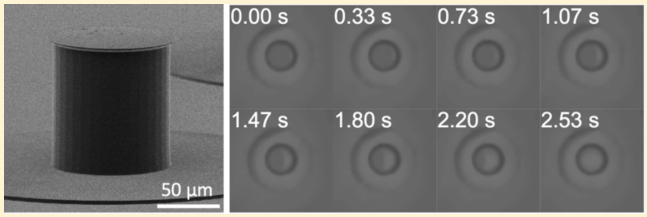

INTRODUCTION

The gecko's exceptional climbing ability on vertical surfaces and ceilings has encouraged extensive scientific investigations on gecko-foot-hair-inspired dry fibrillar adhesives for a decade.[1−4] These synthetic adhesives have been used for a wide range of applications such as manipulation,[5] climbing,[6] and medical applications.[7,8] It has been revealed that the effect of stress distribution on a contact interface plays an important role in achieving higher adhesion.[9,10] Theoretical[11,12] and experimental[13,14] studies on optimal shapes of tip patterns have shown that the stress on the fiber tip should be distributed equally for optimal adhesion. Campo et al. tested various elastomeric fibers with different tip shapes experimentally and found out a mushroomlike fiber tip shape could provide the highest adhesion among many other tip patterns.[15] Effect of the mushroomlike fiber tip ending on improving the maximal adhesion by achieving more uniform stress distribution on the contact interface has been previously studied.[16−19] Recently, Aksak et al. theoretically studied the optimal shape of mushroomlike tip endings of elastomer microfibers as a function of tip diameter relative to stalk diameter (β) and the tip-ending wedge angle (θ) as shown in Figure 1a. They reported β = 1.1−1.2 and θ = 45° as the optimal fiber parameters for the maximal adhesion.[20]

Even though the previous work has already computed the optimal shape of mushroomlike tip endings with maximal adhesion for elastomer microfibrillar structures, they have not been experimentally validated yet due to limitations on the fabrication of three-dimensional (3D) optimal micro/nanostructures. Therefore, in this paper, we experimentally investigated the optimal design of bioinspired elastomer fibrillar structures with mushroom-shaped tip endings to maximize their adhesion. Benefiting from high-resolution 3D two-photon stereo nanolithography techniques, we manufactured elastomer microfibers with different β and θ values precisely to verify such optimal designs. Sixteen different mushroomlike tip patterns were fabricated using two different polyurethanes with different stiffness, and their pull-off forces were compared to the theoretical predictions. Finally, the effect of different tip endings on the adhesion is discussed in terms of the stress distribution and stiffness of the microfibers.

EXPERIMENTAL DETAILS

A schematic of a mushroomlike microfiber is shown in Figure 1a. While we kept the fiber tip diameter (d_t = 100 μm) and the fiber length (L = 100 μm) constant to have the same tip contact area and height for all fiber designs, we varied the tip wedge angle θ and the tip diameter relative to stalk diameter β in the ranges of 30−60° and 1.1−1.5, respectively. Fifteen different designs of mushroomlike tip endings were fabricated, in addition to a cylindrical microfiber that was fabricated as a control fiber. The designed microfibers were fabricated using a UV-curable negative photoresist (IP-Dip, Nanoscribe GmbH), which can be polymerized in any arbitrary 3D shape based on a two-photon polymerization process. Different steps in the fabrication process are shown in Figure 1c. First, we polymerized the IP-Dip at the

Received: July 2, 2015
Revised: August 30, 2015
Published: August 31, 2015

DOI: 10.1021/acs.langmuir.5b02415
Langmuir 2015, 31, 10119−10124

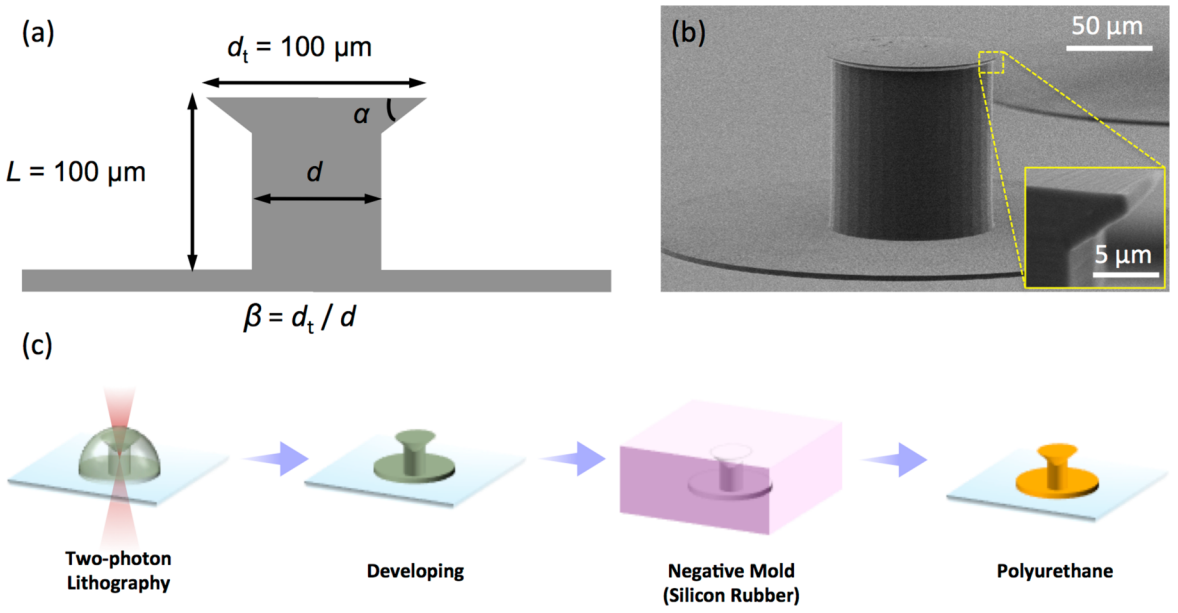

Figure 1. (a) Schematic of a mushroomlike elastomer microfiber. (b) Scanning electron microscope (SEM) image of a 3D-printed microfiber. The inset shows a cross-sectional SEM image of the microfiber tip edge, which is slightly rounded. (c) Fabrication process steps for the microfibers: 3D printing the master fiber from a UV-curable photoresist using two-photon lithography, developing it, creating its negative silicone rubber mold, and molding the negative mold with polyurethane elastomers to create positive fibers.

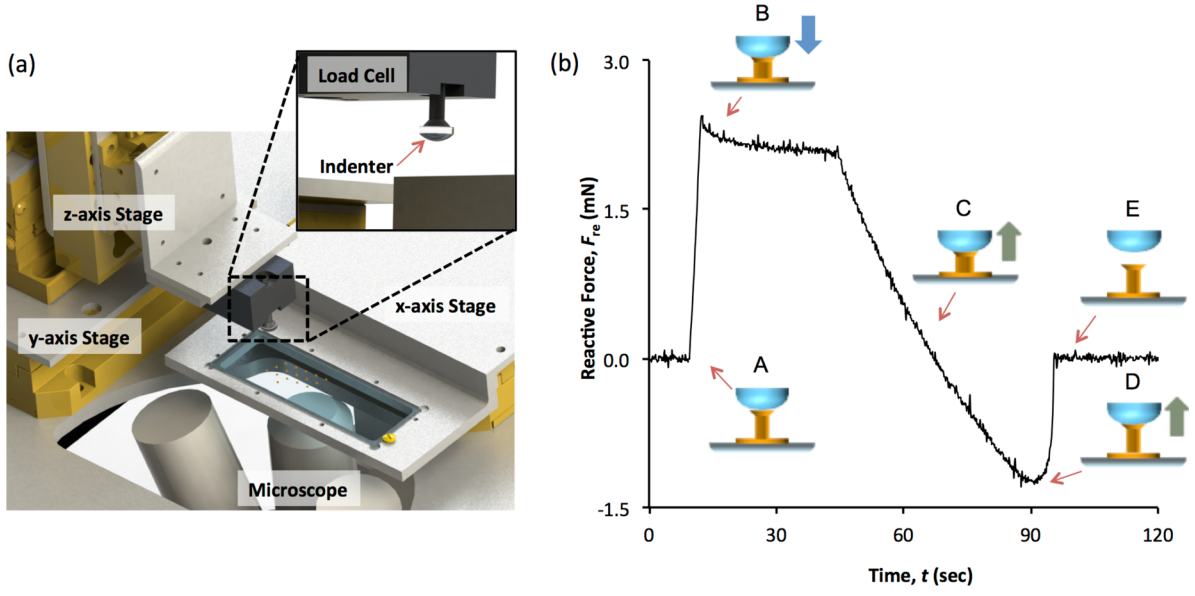

Figure 2. (a) Schematics of the custom automated adhesion characterization setup. A spherical glass indenter is attached to a load cell for vertical force measurement. The load cell is connected to a motorized *XYZ* stage for motion control. An inverted microscope is used to observe the interaction between fiber tips and the spherical indenter. (b) Different steps in the adhesion test shown on a sample force–displacement data plot: (A) The indenter approaches the fiber tip. (B) The indenter makes contact with fiber tip and remains in contact for 30 s. (C) The indenter starts the retraction process. (D) The maximum reactive force is measured. (E) Full tip detachment occurs.

desired shape for positive structures using the two-photon lithography machine (Photonic Professional GT, Nanoscribe GmbH). We then developed the photoresist using 2-methoxy-1-methylethyl acetate (PGMA) and hard baked the fibers at 120 °C for 30 min. Next, we made a negative mold for the fibers using a soft silicon rubber (Mold Max 20, Smooth-On, Inc.; mixed 10:1 by weight). We cured silicon rubber for 24 h at room temperature. We finally fabricated the positive fibers using both ST-1060 polyurethane (BJB Enterprises Inc.; mixed 100:55 by weight) and ST-1087 polyurethane (BJB Enterprises Inc.; mixed 100:50 by weight) elastomers. We degassed polymers 3 min after mixing and 10 min after pouring them on the mold.[21] Two sets of positive fibers for both ST-1060 and ST-1087 polyurethanes were fabricated and cured for 24 h at room temperature followed by 16 h at 71 °C. Figure 1b shows a scanning electron microscope (SEM) image of a sample polymerized master fiber (β = 1.2, θ = 45°). Benefiting from the submicrometer resolution of the two-photon lithography, the shape of the fabricated master fibers had generally good agreement with the original designs while the tip edge was rounded slightly as shown in the inset of Figure 1b. Also, we noticed fabrication defects (broken edge) for the master fiber with β = 1.3 and θ = 30°, and thus we did not perform any experiments with this fiber.

The adhesion of fabricated microfibers was measured with a customized setup shown in Figure 2a that was adapted from our previous work.[21] We used a plano-convex glass indenter with a

DOI: 10.1021/acs.langmuir.5b02415
Langmuir 2015, 31, 10119–10124

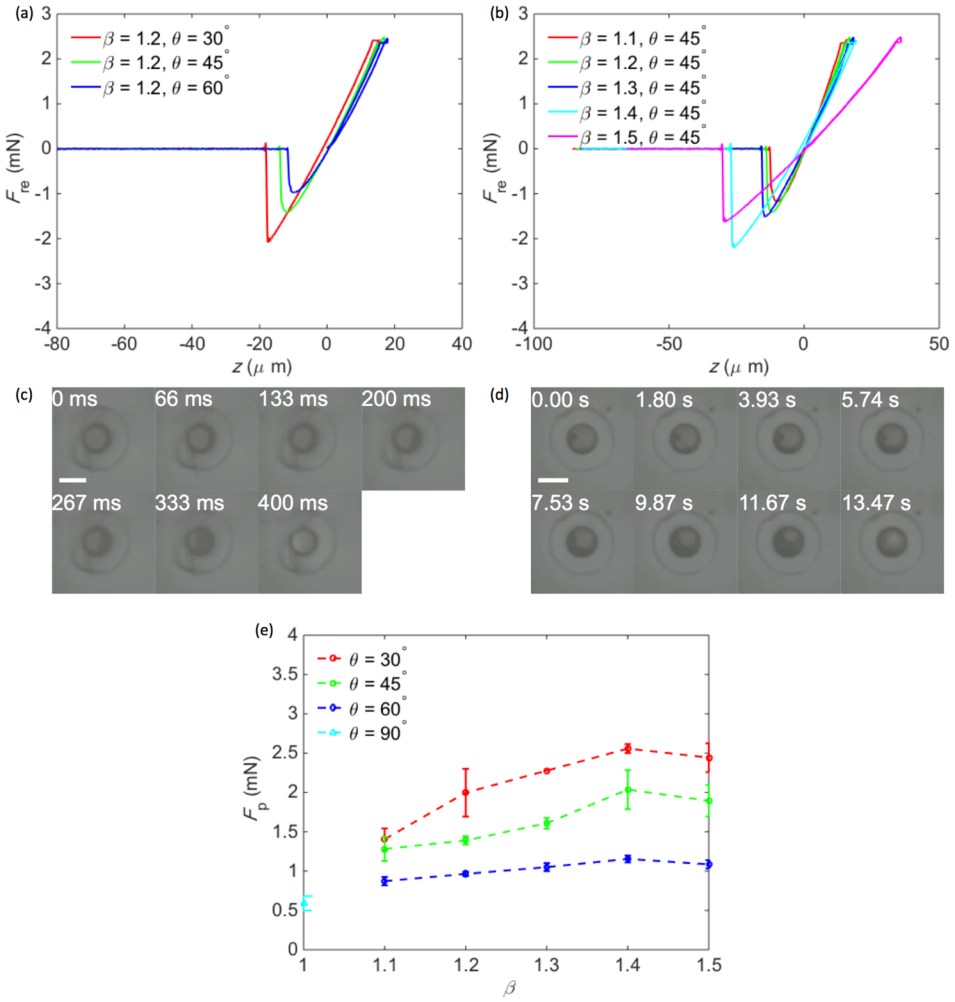

Figure 3. Reactive force F_{re} as a function of displacement z for ST-1060 polyurethane elastomer fibers at (a) $\beta = 1.1$ and $\theta = 30-60°$ and (b) $\theta = 45°$ and $\beta = 1.1-1.5$. Snapshots of crack propagation in ST-1060 fibers at (c) $\theta = 45°$ and $\beta = 1.3$ (optimal) and (d) $\theta = 60°$ and $\beta = 1.2$ (nonoptimal). Scale bars on (c) and (d) correspond to 100 μm. The first images on both (c) and (d) show the crack initiation, and the last images on these parts correspond to full detachment. The entire crack propagation process takes around 400 ms for the optimal set of parameters while it takes around 13.47 s for the nonoptimal case. (e) Experimental pull-off force F_p results in different β and θ values. Each data point is an average of six measurements, and the error bar indicates the standard deviation.

diameter of 6 mm and a radius of curvature of 4.7 mm for our adhesion measurements. Different steps in the adhesion measurement process are illustrated in Figure 2b. We first approached a fiber at a speed of 10 μm/s and preloaded it with 2.5 mN of normal load. Next, we made 30 s of contact with the fiber to make sure the viscoelastic fiber material was relaxed and the contact force was leveled out. We then retracted fiber at 1 μm/s until the indenter was fully detached from the fiber. The pull-off force of each fiber F_p was characterized as the maximum negative reactive force during the retraction step.

RESULTS AND DISCUSSION

Experimental measurements of reactive force F_{re} as a function of vertical displacement z for fibers with $\beta = 1.2$ and $\theta = 30$, 45, and 60° are plotted in Figures 3a and 4a for ST-1060 and ST-1087 polyurethane elastomer fibers, respectively. When applying a preload, the reactive force is shown to be positive, resulting in a positive displacement. With the retraction of the indenter, the reactive force becomes negative, exerting the pull-off force as shown in Figures 3a and 4a. Since the ratio of tip to base diameter β is constant for these samples, slopes of force–displacement curves during the preload are the same for all of them. However, different tip ending wedge angles θ resulted in different pull-off forces; the larger the wedge angle, the lower the pull-off force for this β value. By changing θ from 30 to 60°, the pull-off force on average decreased from 2.00 ± 0.30 to 0.96 ± 0.03 mN for ST-1060 fibers and from 3.75 ± 0.02 to 0.31 ± 0.02 mN for ST-1087 fibers.

As can be seen in Figures 3a and 4a, the larger the pull-off force, the sharper the trough. A sharper trough in this case represents a faster crack propagation and quicker detachment. Such detachment is due to relatively uniform stress distribution, which is one of the main reasons resulting in a higher pull-off force. As shown in Figure 3c,d, the crack propagation time t_d at $\theta = 30°$ and $\beta = 1.4$ resulting in the maximal adhesion for ST-1060 fibers fabricated in this study was around 400 ms. However, the crack propagation time at the minimal pull-off force ($\theta = 60°$ and $\beta = 1.1$) was 13.5 s, approximately 34-fold longer than that of the maximal adhesion. Figure 4c,d illustrates the maximal ($\theta = 30°$ and $\beta = 1.2$, $t_d < 60$ ms) and nonoptimal ($\theta = 45°$ and $\beta = 1.3$, $t_d = 2.5$ s) set of parameters for ST-1087 fibers. As shown in these figures, stiffer fibers made of ST-1087 show higher sensitivity to the shape of wedge angle θ than the softer ST-1060 fibers, approximately a 42-fold difference between the maximal and minimal adhesion.

DOI: 10.1021/acs.langmuir.5b02415
Langmuir 2015, 31, 10119–10124

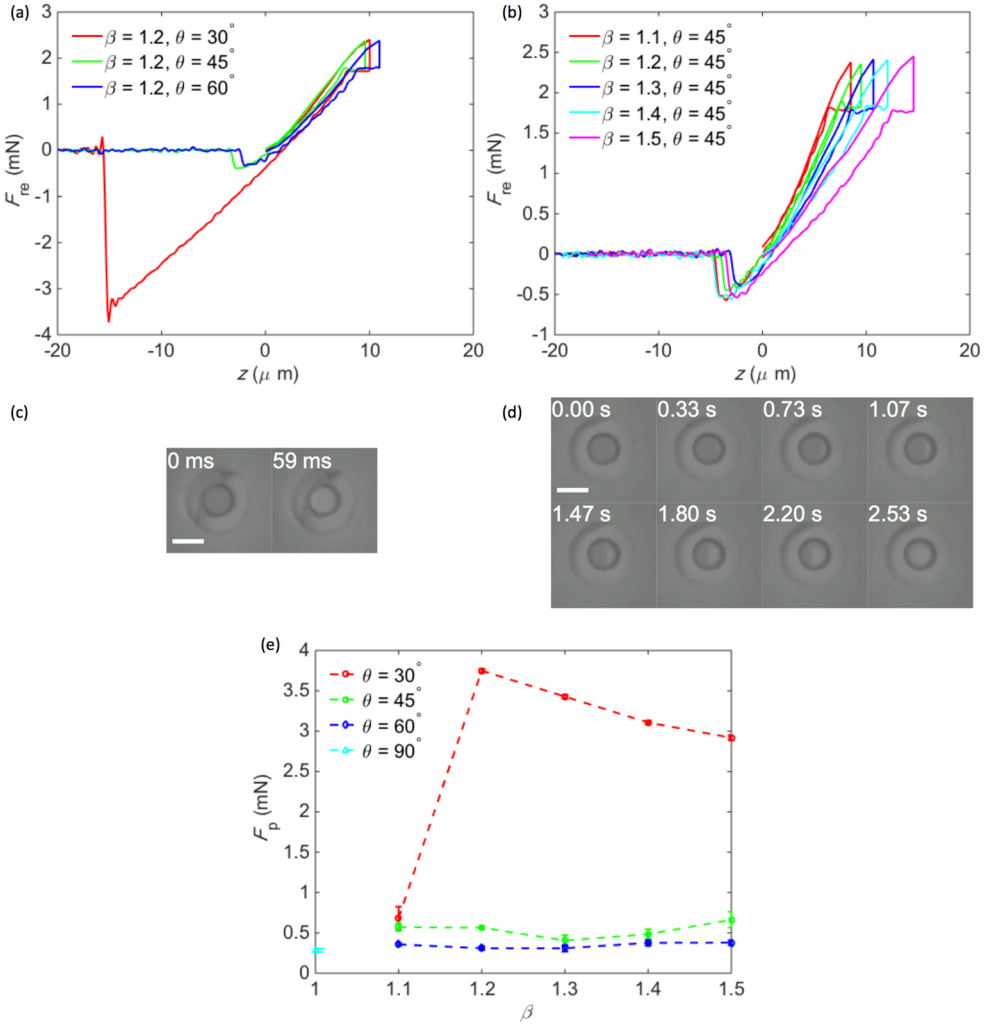

Figure 4. Reactive force F_{re} as a function of displacement z for harder ST-1087 polyurethane elastomer fibers at (a) $\beta = 1.1$ and $\theta = 30–60°$ and (b) $\theta = 45°$ and $\beta = 1.1–1.5$. Snapshots of crack propagation in ST-1087 fibers at (c) $\theta = 30°$ and $\beta = 1.2$ (optimal) and (d) $\theta = 45°$ and $\beta = 1.3$ (nonoptimal). Scale bars on (c) and (d) correspond to 100 μm. The first images on both (c) and (d) show the crack initiation, and the last images on these parts correspond to full detachment. The entire crack propagation process takes less than 60 ms for the optimal set of parameters while it takes around 2.53 s for the nonoptimal case. (e) Experimental pull-off force F_p results in different β and θ values. Each data point is an average of six measurements, and the error bar indicates the standard deviation.

Figures 3b and 4b show the reactive force for $\theta = 45°$ and $\beta = 1.1–1.5$. In this case, the largest pull-off force occurred at $\beta = 1.4$ for ST-1060 ($F_p = 2.04 \pm 0.25$ mN) and $\beta = 1.5$ for ST-1087 ($F_p = 0.66 \pm 0.10$ mN) fibers. Moreover, the larger the β, the smaller the slope of the force–displacement curve. This is mainly due to the decrease in stem diameter and thus its lower stiffness with increasing β. In addition, β also has an impact on stress distribution as illustrated by changes in the sharpness of the troughs in Figures 3b and 4b.[9]

Figures 3e and 4e illustrate pull-off force F_p for fibers with different β and θ values. We used two samples for each combination of β and θ and performed three measurements on each fiber (90 measurements for each material). The measured pull-off force for all ST-1060 fibers ranged from 2.56 ± 0.06 to 0.87 ± 0.05 mN and from 3.75 ± 0.02 to 0.31 ± 0.04 mN for ST-1087 fibers. As shown in Figures 3e and 4e, changing β had different effects depending on the tip-ending wedge angle and the fiber material. The highest theoretical pull-off force for fibers of different β and θ was estimated at $\beta = 1.1–1.2$ and $\theta = 45°$ before.[20] In comparison to the theoretical predictions, approximately similar values for optimal β and θ were observed experimentally ($\theta = 30°$ and $\beta = 1.4$ and 1.2 for ST-1060 and ST-1087 fibers, respectively). One of the possible reasons for the discrepancy between the theoretical predictions and experimental results could be the rounded shape at the edge of the fiber tips, as shown in the inset of Figure 1b. Aksak et al. predicted that even the nanoscale rounded shape of the edge could have a significant impact on the normalized pull-off stress.[20] They also showed that for $\theta = 45°$ there is a lower limit for the pull-off force resulting in a robust adhesion. However, at larger values of θ, there will be a stress singularity at the tip edge resulting in a reduced pull-off force.[20]

According to Tang et al., the normalized pull-off stress $\Phi = \sigma_s/\sigma_0$ (σ_s is the pull-off stress and σ_0 is the theoretical strength of the interface, which could be in between $E/10$ and $E/5$ where E is the elastomer material's Young's modulus[22]) of a soft elastic cylindrical fiber that is in contact with a flat rigid surface depends on dimensionless parameter χ as[23]

$$\chi = \frac{\sigma_0^2 a(1-\nu^2)}{2\pi E w_{adh}} \quad (1)$$

DOI: 10.1021/acs.langmuir.5b02415
Langmuir 2015, 31, 10119–10124

where a is the fiber stem radius, ν is the fiber Poisson ratio, and w_{adh} is the work of adhesion at the fiber−surface interface. In our study, χ was between 2 and 3 for soft ST-1060 fibers and between 20 and 30 for stiff ST-1087 fibers. Figure 5a,b shows

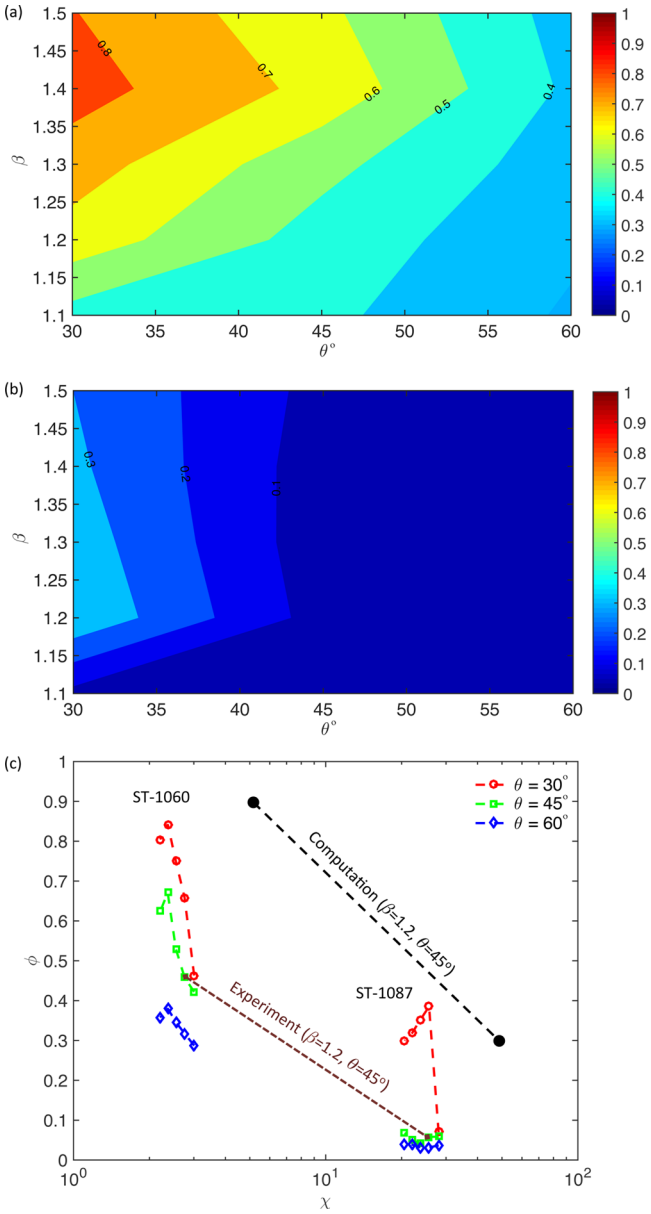

Figure 5. Contour plots of normalized experimental pull-off stress Φ values as a function of β and θ for (a) ST-1060 and (b) ST-1087 mushroomlike polyurethane elastomer fibers. (c) Φ versus χ for both ST-1060 and ST-1087 fibers at different wedge angles. The black and brown dashed lines compare the decrease in Φ with increasing χ for computational results versus experimental measurements.

that soft ST-1060 fibers could achieve a higher normalized pull-off stress Φ than stiff ST-1087 fibers over the entire range of different β and θ values. Also, as predicted by Aksak et al., at the rounded edge shown in the inset of Figure 1b, Φ was observed to decrease with increasing χ, as shown in Figure 5c.[20] We should note that even though Φ of the stiff fibers is much smaller than that of the soft fibers, the actual pull-off force of stiff fibers was higher than that of the soft fibers due to the high theoretical strength of the interface σ_0, implying that the stiffer material could be better for higher adhesion strength if we could more precisely fabricate the optimal tip ending shape of microfibers and achieve full tip contact on the surface.

OUTLOOK

Theoretical studies of optimal adhesion for bioinspired mushroomlike fibers have shown the significance of tip diameter relative to stalk diameter (β) and the tip-ending wedge angle (θ).[20] However, there has been no experimental verification of such studies due to issues related to the precise fabrication of 3D mushroomlike fiber tip endings with controlled β and θ. In this study, we used 3D nanolithography techniques to fabricate polyurethane elastomer mushroomlike fibers with different β and θ values. Conducting measurements of single fiber adhesion, we found that changing β at each θ affects the slope of the force−displacement curve as a result of changes in fiber stiffness; the higher the β, the lower the slope of this curve. Moreover, θ had a significant impact on the sharpness of the troughs on force−displacement curves and thus on crack propagation, which is mainly due to different stress distributions at different values of θ (although β also has an impact on the stress distribution by changing the fiber stiffness).[9] θ = 30° resulted in the sharpest troughs and fastest crack propagation (for both tested polyurethane elastomer materials) due to a relatively uniform stress distribution. In addition, we found the maximal pull-off force at θ = 30° and β = 1.4 and 1.2 for ST-1060 and ST-1087, respectively. The discrepancy between the computational estimation and experimental results could be mainly due to the rounded shape at the edge of the microfibers as predicted by Aksak et al.[20] The proposed fabrication technique could be used to fabricate many other complex microstructured adhesive designs on a similar scale with high precision. With the adhesion characterization setup used in this study, we can measure their adhesive force and investigate their optimality. Thus, arrays of microfibers with such optimal tip endings could be fabricated and used in a wide range of repeatable adhesive applications in robotics, consumer products, manufacturing, medical and electronic devices, and so forth requiring strong pull-off or peel strength.

AUTHOR INFORMATION

Corresponding Author

*E-mail: sitti@is.mpg.de.

Author Contributions

The manuscript was written through the contributions of all authors. All authors have given approval to the final version of the manuscript. H.M. and S.S. contributed equally.

Notes

The authors declare no competing financial interest.

ACKNOWLEDGMENTS

We thank the National Science Foundation (grant no. CMMI-1130520) for funding and members of the NanoRobotics Lab and Mats Forssell for helpful comments.

REFERENCES

(1) Autumn, K.; Liang, Y. A.; Hsieh, S. T.; Zesch, W.; Chan, W. P.; Kenny, T. W.; Fearing, R.; Full, R. J. Adhesive force of a single gecko foot-hair. *Nature* **2000**, *405*, 681−685.

DOI: 10.1021/acs.langmuir.5b02415
Langmuir 2015, 31, 10119−10124

(2) Geim, A. K.; Dubonos, S. V.; Grigorieva, I. V.; Novoselov, K. S.; Zhukov, A. A.; Shapoval, S. Y. Microfabricated adhesive mimicking gecko foot-hair. *Nat. Mater.* **2003**, *2*, 461−463.
(3) Arzt, E.; Gorb, S.; Spolenak, R. From micro to nano contacts in biological attachment devices. *Proc. Natl. Acad. Sci. U. S. A.* **2003**, *100*, 10603−10606.
(4) Glassmaker, N. J.; Jagota, A.; Hui, C.; Noderer, W. L.; Chaudhury, M. K. Biologically inspired crack trapping for enhanced adhesion. *Proc. Natl. Acad. Sci. U. S. A.* **2007**, *104*, 10786−10791.
(5) Song, S.; Sitti, M. Soft Grippers Using Micro-fibrillar Adhesives for Transfer Printing. *Adv. Mater.* **2014**, *26* (28), 4901−4906.
(6) Kim, S.; Spenko, M.; Trujillo, S.; Heyneman, B.; Mattoli, V.; Cutkosky, M. R. Whole body adhesion: hierarchical, directional and distributed control of adhesive forces for a climbing robot. *IEEE Int. Conf. Rob. Autom.* **2007**, 1268−1273.
(7) Mahdavi, A.; Ferreira, L.; Sundback, C.; Nichol, J. W.; Chan, E. P.; Carter, D. J.; Karp, J. M. A biodegradable and biocompatible gecko-inspired tissue adhesive. *Proc. Natl. Acad. Sci. U. S. A.* **2008**, *105* (7), 2307−2312.
(8) Kwak, M. K.; Jeong, H. K.; Suh, K. Y. Rational design and enhanced biocompatibility of a dry adhesive medical skin patch. *Adv. Mater.* **2011**, *23* (34), 3949−3953.
(9) Aksak, B.; Hui, C.; Sitti, M. Effect of aspect ratio on adhesion for soft elastic fibers. *J. R. Soc., Interface* **2011**, *8*, 1166−1175.
(10) Spuskanyuk, A. V.; McMeeking, R. M.; Deshpande, V. S.; Arzt, E. The effect of shape on the adhesion of fibrillar surfaces. *Acta Biomater.* **2008**, *4*, 1669−1676.
(11) Gao, H.; Yao, H. Shape insensitive optimal adhesion of nanoscale fibrillar structures. *Proc. Natl. Acad. Sci. U. S. A.* **2004**, *101* (21), 7851−7856.
(12) Tsang, P. H.; Li, G.; Brun, Y. V.; Freund, L. B.; Tang, J. X. Adhesion of single bacterial cells in the micronewton range. *Proc. Natl. Acad. Sci. U. S. A.* **2006**, *103* (15), 5764−5768.
(13) Sameoto, D.; Sharif, H.; Menon, C. Investigation of low-pressure adhesion performance of mushroom shaped biomimetic dry adhesives. *J. Adhes. Sci. Technol.* **2012**, *26* (23), 2641−2652.
(14) Wang, Y.; Shao, J.; Ding, Y.; Li, X.; Tian, H.; Hu, H. Effects of contact cap dimension on dry adhesion of bioinspired mushroom-shaped surfaces. *Proc. SPIE* **2015**, *9429*, 94291E−94291E-6.
(15) del Campo, A.; Greiner, C.; Arzt, E. Contact shape controls adhesion of bioinspired fibrillar surfaces. *Langmuir* **2007**, *23*, 10235−10243.
(16) Heepe, L.; Kovalev, A. E.; Filippov, A. E.; Gorb, S. N. Adhesion failure at 180,000 frames per second: Direct observation of the detachment process of a mushroom-shaped adhesive. *Phys. Rev. Lett.* **2013**, *111* (10), 104301.
(17) Heepe, L.; Gorb, S. N. Biologically inspired mushroom-shaped adhesive microstructures. *Annu. Rev. Mater. Res.* **2014**, *44*, 173−203.
(18) Carbone, G.; Pierro, E. Sticky bio-inspired micropillars: Finding the best shape. *Small* **2012**, *8* (9), 1449−1454.
(19) Carbone, G.; Pierro, E. Origin of the superior adhesive performance of mushroom-shaped microstructured surfaces. *Soft Matter* **2011**, *7* (12), 5545−5552.
(20) Aksak, B.; Sahin, K.; Sitti, M. The optimal shape of elastomer mushroom-like fibers for high and robust adhesion. *Beilstein J. Nanotechnol.* **2014**, *5*, 630−638.
(21) Marvi, H.; Han, Y.; Sitti, M. Actively controlled fibrillar friction surfaces. *Appl. Phys. Lett.* **2015**, *106* (5), 051602.
(22) Maugis, D. *Contact, Adhesion, and Rupture of Elastic Solids*; Springer Verlag: Berlin, 2000.
(23) Tang, T.; Hui, C. Y.; Glassmaker, N. J. Can a fibrillar interface be stronger and tougher than a non-fibrillar one? *J. R. Soc., Interface* **2005**, *2* (5), 505−516.

DOI: 10.1021/acs.langmuir.5b02415
Langmuir 2015, 31, 10119−10124